Author Manuscript

Author Manuscript

Author Manuscript

Author Manuscript

HHS Public Access

Author manuscript

NMR Biomed. Author manuscript; available in PMC 2018 December 01.

Published in final edited form as:

NMR Biomed. 2017 December ; 30(12): . doi:10.1002/nbm.3786.

^{31}P Magnetic Resonance Fingerprinting for Rapid Quantification of Creatine Kinase Reaction Rate In Vivo

Charlie Y. Wang[1], **Yuchi Liu**[1], **Shuying Huang**[1], **Mark A. Griswold**[1,2], **Nicole Seiberlich**[1,2], and **Xin Yu**[1,2,3]

[1]Department of Biomedical Engineering, Case Western Reserve University, Cleveland, Ohio

[2]Department of Radiology, Case Western Reserve University, Cleveland, Ohio

[3]Department of Physiology and Biophysics, Case Western Reserve University, Cleveland, Ohio

Abstract

Purpose—To develop a ^{31}P spectroscopic magnetic resonance fingerprinting (MRF) method for fast quantification of the chemical exchange rate between phosphocreatine (PCr) and ATP via creatine kinase (CK).

Methods—A ^{31}P MRF sequence (CK-MRF) was developed to quantify the forward rate constant of ATP synthesis via CK (k_f^{CK}), the T_1 relaxation time of PCr (T_1^{PCr}), and the PCr-to-ATP concentration ratio (M_R^{PCr}). The CK-MRF sequence used a bSSFP-type excitation with ramped flip angles and a unique saturation scheme sensitive to the exchange between PCr and γATP. Parameter estimation was accomplished by matching the acquired signals to a dictionary generated using the Bloch-McConnell equation. Simulation studies were performed to examine the susceptibility of the CK-MRF method to several potential error sources. The accuracy of nonlocalized CK-MRF measurements before and after an ischemia-reperfusion (IR) protocol was compared to magnetization transfer (MT-MRS) method in rat hindlimb at 9.4 T (n=17). Reproducibility of CK-MRF was also assessed by comparing CK-MRF measurements to both MT-MRS (n=17) and four angle saturation transfer (FAST) methods (n=7).

Results—Simulation results showed that CK-MRF quantification of k_f^{CK} was robust with <5% error in the presence of model inaccuracies including dictionary resolution, metabolite T_2 values, P_i metabolism, and B_1 miscalibration. Estimation of k_f^{CK} by CK-MRF (0.38±0.02 s^{-1} at baseline and 0.42±0.03 s^{-1} post-IR) showed strong agreement with MT-MRS (0.39±0.03 s^{-1} at baseline and 0.44±0.04 s^{-1} post-IR). k_f^{CK} estimation was also similar between CK-MRF and FAST (0.38±0.02 s^{-1} for CK-MRF and 0.38±0.11 s^{-1} for FAST). The coefficient of variation from 20-s CK-MRF quantification of k_f^{CK} was 42% of that by 150-s MT-MRS acquisition and was 12% of that by 20-s FAST acquisition.

Conclusion—This study demonstrates the potential of a ^{31}P spectroscopic MRF framework for rapid, accurate and reproducible quantification of chemical exchange rate of CK *in vivo*.

*Address correspondence to: Xin Yu, Sc.D., Wickenden 430, 10900 Euclid Avenue, Cleveland, OH, 44106, Tel: 216-368-3918, Fax: 216-368-4969, xin.yu@case.edu.

Author Manuscript Author Manuscript Author Manuscript Author Manuscript

Graphical Abstract

A ^{31}P spectroscopic pulse sequence based on magnetic resonance fingerprinting framework was designed to quantify the forward rate constant of ATP synthesis via creatine kinase. Simulation results demonstrated the robustness of this method to several sources of experimental errors. In vivo studies on rat hindlimb showed significantly higher reproducibility than conventional magnetization transfer method with only 13% of the acquisition time.

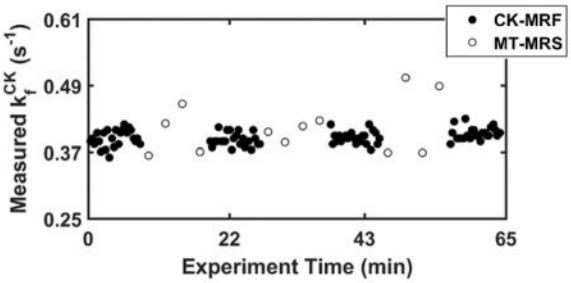

Keywords

magnetic resonance fingerprinting; ^{31}P spectroscopy; creatine kinase metabolism; ischemia/reperfusion

Introduction

Magnetic Resonance Spectroscopy (MRS) offers a unique opportunity to noninvasively characterize metabolic profiles due to its chemical specificity. Phosphorus-31 (^{31}P) MRS has been used extensively to assess the energetics of living tissues[1–4]. In addition to measuring tissue concentrations of phosphate metabolites, ^{31}P magnetization transfer (MT) techniques using saturation transfer[5] or inversion transfer[6,7] have been developed to quantify the phosphocreatine (PCr) synthesis rate via creatine kinase (CK) in heart, skeletal muscle, and brain[8–15]. However, due to the low concentrations of phosphate metabolites, MT-MRS methods typically require long acquisition time to achieve adequate signal-to-noise ratio (SNR).

Shorter acquisition times have been achieved previously by using a combination of two strategies for CK measurements. The first strategy uses a reduced number of spectra acquired under partially relaxed conditions, such as in the Four Angle Saturation Transfer (FAST) method[16], or the Triple Repetition Time Saturation Transfer (TRiST) method[17]. Reducing the number of acquired spectra is particularly useful in combination with chemical shift imaging (CSI) methods for spatially localized measurements. The second strategy further reduces the number of acquired spectra by assuming an intrinsic T_1 value for PCr. These methods include the Two Repetition Time Saturation Transfer (TwiST)[18] and T_1 Nominal[19] methods.

The Magnetic Resonance Fingerprinting (MRF) technique is a new framework to potentially reduce the time needed for quantitative measurements. MRF extracts parameter maps from signals generated using non-steady state pulse sequences in conjunction with Bloch

Author Manuscript Author Manuscript Author Manuscript Author Manuscript

simulations and pattern matching. This parameter estimation framework allows for greater flexibility in pulse sequence design than conventional methods and has been successfully utilized for efficient measurement of proton (^{1}H) relaxation times in the brain[20,21], abdomen[22], and heart[23].

In this work, a new fast and robust ^{31}P CK-MRF measurement strategy is proposed using the MRF framework. While the technique is based on the original MRF pulse sequence and dictionary matching method, several additional strategies to improve the sensitivity to chemical exchange via CK have been incorporated. First, a ^{31}P bSSFP-type sequence[24] with a ramped flip angle series[25] was employed to improve SNR efficiency. Second, selective saturation pulses and excitation pulses were rapidly alternated to allow simultaneous encoding of chemical exchange and sampling of transient signal evolution. The accuracy and robustness of this method were first evaluated in simulation studies in which several potential error sources were assessed. *In vivo* studies on rat hindlimb were performed to validate the CK-MRF measurements against a conventional ^{31}P magnetization transfer (MT-MRS) method. Finally, a reproducibility comparison between the proposed CK-MRF method and the MT-MRS and FAST methods was performed.

Materials and Methods

Pulse Sequence

A schematic of the CK-MRF pulse sequence is shown in Figure 1a. Following an inversion preparation, a bSSFP-type acquisition scheme for ^{31}P spectroscopy was employed. The acquisition was made up of a total of 32 acquisition blocks. To enable accurate quantification of PCr and γATP signals, two types of acquisition blocks, ACQ-PCr and ACQ-γATP, were used to acquire signals from PCr and γATP, respectively. A 490-ms selective saturation block was used between two acquisition blocks, with the saturation frequency set either at the resonance frequency of γATP (SAT-γATP) or at the frequency contralateral to γATP (SAT-CNTL). The entire acquisition is comprised of two modules that employed SAT-CNTL and SAT-γATP, respectively, with the two acquisition blocks for PCr and γATP alternated eight times in each module.

Diagrams of acquisition blocks for ACQ-PCr and ACQ-γATP are shown in Figures 1b and 1c. Each block consisted of a train of 10 linearly ramped-up and ramped-down excitations with alternating phase and a constant TR of 12.8 ms. Selective excitation was performed with a 4 ms Gaussian pulse centered at the resonance frequency of PCr and γATP, respectively. Following each excitation, 7.7 ms of FID signal was acquired with 256 data points, resulting in a spectral resolution of 130 Hz/pt.

The nominal flip angle, frequency, and timing of all 320 RF excitations for CK-MRF are shown in Figure 1d. The maximum flip angles in the 32 acquisition blocks were modulated by a sinusoidal envelope. The total time for one complete CK-MRF acquisition was 20 s. Multiple repetitions were acquired with no delay, with a single dummy acquisition preceding each series of repetitions.

Author Manuscript Author Manuscript Author Manuscript Author Manuscript

Fingerprint Simulation

Signal time courses, i.e. the fingerprints, were simulated by solving the modified Bloch-McConnell equation[16,26] with two exchanging pools, i.e., PCr, and γATP. Details of the simulation methods are described in the Appendix. Simulation of a fingerprint required a total of nine input parameters: the forward rate constant of ATP synthesis via CK (k_f^{CK}), the concentration ratio of PCr-to-ATP (M_R^{PCr}), the T_1 and T_2 relaxation times and the resonance frequencies (chemical shift) of PCr and γATP ($T_1^{\mathrm{PCr}}, T_1^{\gamma\mathrm{ATP}}, T_2^{\mathrm{PCr}}, T_2^{\gamma\mathrm{ATP}}$, ω^{PCr}, $\omega^{\gamma\mathrm{ATP}}$), as well as B_0 distribution characterized by a linewidth, LW. Given a set of input parameters, spin evolution was simulated in sequential time steps, starting from a fully relaxed initial condition. Excitation was simulated by discretizing the Gaussian shaped RF pulse into 41 instantaneous complex rotations (Equations A7–9), with the magnitude of the rotation following a Gaussian envelope, and the total rotation summing to the nominal FA. The phase of each rotation was determined by the excitation frequency. γATP saturation was simulated by instantaneous saturation of γATP magnetization with no direct effect on PCr magnetization. The pulse sequence was simulated sequentially twice to account for the dummy scan. For each simulation, all FID signals were recorded from the bulk transverse magnetization, described as $S(t)$ in Equation A12.

Dictionary Generation

The dictionary in the MRF framework is a set of fingerprints, or signal evolutions, for selected values of the tissue properties. Four tissue properties, namely $k_f^{\mathrm{CK}}, T_1^{\mathrm{PCr}}$, ω^{PCr}, and M_R^{PCr}, were varied over their physiologically expected range to generate a dictionary for template matching. Specifically, 51 values of k_f^{CK} ranging from 0.3 to 0.55 s^{-1} with a resolution of 0.005 s^{-1}, 20 values of T_1^{PCr} uniformly distributed from 2.8 to 4.7 s, 11 values for ω^{PCr} spanning from −15 to 15 Hz, and 49 values for M_R^{PCr} uniformly distributed from 3.0 to 5.4 were simulated. It is worth noting that these ranges of parameter variations reflect physiological variations expected in the current study and may need to be expanded for other studies. $\omega^{\gamma\mathrm{ATP}}$ for each entry was constrained to ($\omega^{\mathrm{PCr}} - \Delta\omega^{\mathrm{PCr}-\gamma\mathrm{ATP}}$), where $\Delta\omega^{\mathrm{PCr}-\gamma\mathrm{ATP}}$ was the chemical shift difference between PCr and γATP and was fixed at 2.4 ppm. The remaining 4 parameters, $T_1^{\gamma\mathrm{ATP}}, T_2^{\mathrm{PCr}}, T_2^{\gamma\mathrm{ATP}}$, and LW, were set at 120 ms, 16 ms, 0.8 s, and 15 Hz respectively based on pilot data. $T_1^{\gamma\mathrm{ATP}}$ value was corrected to compensate for nuclear Overhauser effect (NOE)[6,27] from αATP and βATP.

Parameter Matching

Matching was performed in the frequency domain to reduce memory load. Each of the 320 FIDs, for all acquired data and simulated dictionary entries, was Fourier transformed, and the complex-valued data points corresponding to PCr or γATP resonances in these spectra were selected. This resulted in a time course signal, the fingerprint, showing the evolution of PCr and γATP peaks. The inner products between the normalized fingerprint and all entries of the normalized dictionary were computed. The dictionary entry that produced the largest magnitude of the inner product was considered to be the best match. From this match, the

Author Manuscript Author Manuscript Author Manuscript Author Manuscript

values of $k_f^{\mathrm{CK}}, T_1^{\mathrm{PCr}}$, ω^{PCr}, and M_R^{PCr} were derived. Subsequently, the spin density of γATP ($M_0^{\gamma\mathrm{ATP}}$) was computed as the scale factor between the fingerprint and its matched dictionary entry. All data processing and parameter estimation were fully automated.

Conventional MT-MRS

Conventional MT-MRS method was used for validation and comparison. MT-MRS acquisition consisted of 9 spectra: 7 spectra acquired after γATP saturation, with saturation times of 0.4, 0.9, 1.3, 2.2, 3.5, 5.3 and 7 s, respectively; a control spectrum with contralateral saturation; and a conventional spectrum without saturation[19]. All spectra were acquired using 90° hard pulses (130-μs duration) and a 16-s TR. Saturation was accomplished by applying continuous wave RF to the frequency of saturation. Post-processing consisted of 15 Hz line broadening, Fourier transform, and correction of phase and baseline. For phase correction, zero- and first-order phase correction values were obtained manually from spectrum with 12 signal averages and no γATP saturation. These phase correction values were applied to all the spectra acquired from the same animal. The phase correction was followed by automated baseline correction. The signal intensity from PCr was quantified by integrating the area under the PCr peak. Subsequently, $k_f^{\mathrm{CK}}, T_1^{\mathrm{PCr}}$, and M_0^{PCr} were determined by fitting the explicit solution of the Bloch-McConnell equation to the experimental data[28]. Effects of RF spillover were corrected using the method outlined by Kingsley and Monahan[29].

FAST Method

The reproducibility and efficiency of the CK-MRF measurements were also compared with the FAST method. The FAST acquisition consisted of 4 spectra acquired with either 15° or 60° FA, and with either γATP or control saturation[16]. A BIR-4 pulse was used for excitation. All the spectra were acquired after five dummy scans with a TR of 1 s. Parameter estimation of $k_f^{\mathrm{CK}}, T_1^{\mathrm{PCr}}$, and M_R^{PCr} for FAST data was performed using the established closed-form derivation.

Simulations Studies

Performance of Parameter Quantification using Dictionary-Based Approach— Simulations were performed to assess the potential errors in parameter quantification caused by using a finite dictionary resolution. A total of 1000 sets of $k_f^{\mathrm{CK}}, T_1^{\mathrm{PCr}}$, ω^{PCr}, and M_R^{PCr} values were randomly generated with upper and lower bounds consistent with the dictionary's ranges. The remaining 5 input parameters, i.e., $\omega^{\gamma\mathrm{ATP}}$, $T_2^{\mathrm{PCr}}, T_2^{\gamma\mathrm{ATP}}, T_1^{\gamma\mathrm{ATP}}$, and LW were fixed, with $\omega^{\gamma\mathrm{ATP}}$ constrained to (ω^{PCr} – 2.4) ppm. Test fingerprints were generated by simulation of the CK-MRF pulse sequence for each set of parameter values and were matched against the dictionary. The matching errors were calculated as the difference between the matched parameters and the parameters used in simulation.

Sensitivity of Parameter Quantification to Fixed Parameter Values—Since five parameters ($\Delta\omega^{\mathrm{PCr-}\gamma\mathrm{ATP}}$, $T_2^{\mathrm{PCr}}, T_2^{\gamma\mathrm{ATP}}, T_1^{\gamma\mathrm{ATP}}$, and LW) were not varied in the dictionary,

Author Manuscript Author Manuscript Author Manuscript Author Manuscript

errors in their values may affect the accuracy of the matched parameters. Simulations were performed to assess how incorrect selection of the fixed parameters could influence the matched parameters. In addition to these five parameters, the impact of a constant B_1 scale error, resulting in a consistent error in flip angles, was also evaluated. First, a test parameter set (800, 3700, 16 and 120 ms for $T_1^{\gamma\mathrm{ATP}}$, T_1^{PCr}, $T_2^{\gamma\mathrm{ATP}}$, and T_2^{PCr}, −389 and 0 Hz for $\omega^{\gamma\mathrm{ATP}}$ and ω^{PCr}, 0.42 s^{-1} for k_f^{CK}, 4.1 for M_R^{PCr}, and 15 Hz LW, respectively) was chosen to evaluate how errors in the fixed parameters could alter dictionary matching results. To assess the impact of using the wrong values for fixed parameters, test fingerprints were generated by varying the values of a fixed parameter and subsequently matched to the dictionary generated using the test parameter set. The potential impact of each fixed parameter was assessed by calculating the difference between the matched parameters and the true test parameter values. Error calculations for T_2^{PCr}, $T_2^{\gamma\mathrm{ATP}}$, $T_1^{\gamma\mathrm{ATP}}$ were performed by varying each parameter between 50% and 150% of its test value. Error calculations for $\Delta\omega^{\mathrm{PCr}-\gamma\mathrm{ATP}}$ used a range of −430 to −349 Hz. Error calculations for B_1 were performed by scaling all flip angles to between 50% and 150% of their nominal values.

In addition to error analyses, the effect of P_i-to-ATP exchange on parameter estimation, as well as the errors associated with using contralateral saturation to correct for the spillover effect of the γATP saturation on PCr, were also evaluated by simulation (See Supplemental Methods and Figures).

In Vivo Study Protocol

In vivo studies were performed to assess the accuracy of the CK-MRF measurements in rat hindlimb. Details of the experimental setup have been described previously[30]. Briefly, three-month-old Sprague-Dawley rats (n=21) were anesthetized and positioned laterally in a cradle. The hindlimb was secured within a 15-mm ^{31}P saddle coil placed within a ^{1}H volume coil and positioned at the isocenter of a 9.4T MRI scanner (Bruker Biospin Co., Billerica, MA). An air pressure cuff was placed proximal to the coil. Body temperature was maintained at above 35°C via a feedback control system (SA Instruments, Stony Brook, New York, USA). The respiratory rate was maintained between 45 and 60 breaths per minute by manually adjusting the anesthesia level. The animal protocol was approved by the Institutional Animal Care and Use Committee of Case Western Reserve University.

Following initial stabilization, shimming, and B_1 power calibrations, CK-MRF and MT-MRS data were acquired at baseline. Due to their substantially different acquisition times for a single-average dataset (20 s for CK-MRF versus 150 s for MT-MRS), 24 repetitions of CK-MRF data (8 min acquisition) and 4 repetitions of MT-MRS data (10 min acquisition) were acquired in an interleaved manner. A total of 96 repetitions of CK-MRF data and 12 repetitions of MT-MRS data were acquired. 14 rats subsequently underwent two rounds of ischemia/reperfusion (IR) before a second data collection session. Ischemia was induced by inflating the cuff to above 200 mmHg and lasted for 17 min. The ischemic period was followed by 17 minutes of reperfusion. At the end of the IR protocol, another session of data collection started, in which a total of 48 repetitions of CK-MRF data and 8 repetitions of MT-MRS data were acquired.

Author Manuscript Author Manuscript Author Manuscript Author Manuscript

High SNR signals were obtained by averaging all repetitions from a data acquisition session in data analysis. For CK-MRF, this amounted to 96 and 48 averages for data acquired at baseline and post-IR, corresponding to a total acquisition time of 32 and 16 min, respectively. For MT-MRS, the number of signal averages was 12 and 8 at baseline and post-IR, corresponding to 30- and 20-min acquisition, respectively.

Three rats were used as the controls. They underwent the same data collection sessions, separated by a 70-min period, during which CK-MRF and FAST data were collected. An additional 4 rats were also used for the comparison between CK-MRF and FAST methods. Acquisition of 24 repetitions of CK-MRF data and 120 repetitions of FAST data were interleaved, corresponding to approximately 8-min acquisition for each method. A total of 96 and 480 repetitions were collected for the CK-MRF and FAST methods, respectively.

Statistical Analysis

All data processing, simulations, and statistical analysis were performed by custom-built software written in Matlab (Mathworks, Natick, MA). All results are presented as mean ± SD. Bland-Altman plot was used to compare CK-MRF and MT-MRS measurements with high SNR. The coefficient of variation (CV) of an estimated parameter, calculated as the ratio of the standard deviation to the mean, was used to assess the reproducibility. Two-tailed paired Student's *t*-test was used to determine the significance of any observed differences between the CK-MRF and MT-MRS or FAST methods, or before and after IR. Two-tailed unpaired Student's *t*-test were used to determine the significance of differences observed following IR compared to controls, as well as the differences between coefficients of variation in reproducibility study. A p value less than 0.05 was considered significant.

Results

Performance of Parameter Quantification using Dictionary Based Approach

Figure 2 shows the performance of the dictionary approach for parameter quantification. The average errors for matched parameters were 0.0014 s^{-1} for the forward rate constant of CK (k_f^{CK}), 0.03 s for T_1 of PCr (T_1^{PCr}), 0.74 Hz for chemical shift of PCr (ω^{PCr}), and 0.014 for PCr-to-ATP ratio (M_R^{PCr}). The worst case error for each parameter was 0.006 s^{-1} for k_f^{CK}, 0.129 s for T_1^{PCr}, 1.55 Hz for ω^{PCr}, and 0.049 for M_R^{PCr}. With the exception of T_1^{PCr}, these errors were approximately one half of the dictionary step for each parameter.

Sensitivity of Parameter Quantification to Fixed Parameter Values

Figure 3 shows the effects of discrepancies in fixed parameters on the accuracy of the estimation of $T_1^{\mathrm{PCr}}, k_f^{\mathrm{CK}}, M_R^{\mathrm{PCr}}$, and $M_0^{\gamma\mathrm{ATP}}$. No error in ω^{PCr} was observed in any of the tested ranges. Discrepancies in $T_1^{\gamma\mathrm{ATP}}, T_2^{\gamma\mathrm{ATP}}$, and B_1 resulted in errors with various degrees in the matched parameters. Specifically, overestimation of $T_1^{\gamma\mathrm{ATP}}$ caused underestimation of k_f^{CK} and $M_0^{\gamma\mathrm{ATP}}$ and overestimation of M_R^{PCr} (Figure 3a). Errors in $T_2^{\gamma\mathrm{ATP}}$ led to less than 5% error in matched k_f^{CK} for the range investigated but resulted in

Author Manuscript Author Manuscript Author Manuscript Author Manuscript

errors primarily in M_R^{PCr} and $M_0^{\gamma\mathrm{ATP}}$ (Figure 3b). A miscalibration in B_1 power resulted in significant errors in matched T_1^{PCr} and $M_0^{\gamma\mathrm{ATP}}$ but minimally affected k_f^{CK} and M_R^{PCr} (Figure 3c). Finally, errors in $\Delta\omega^{\mathrm{PCr}-\gamma\mathrm{ATP}}$, T_2^{PCr} and LW caused relatively small errors in all matched parameters (Figure 3d–f).

Sensitivity of Parameters Quantification to P_i-to-ATP Exchange

Figure 1S shows the matching errors caused by using a two-pool exchange model. The effects of P_i-to-ATP exchange on the accuracy of the matched parameters were evaluated by increasing both the forward rate constant of P_i-to-ATP (k_f^{Pi}, Figure 1Sa) and the P_i-to-ATP concentration ratio (M_R^{Pi}, Figure 1Sb). At the current dictionary resolution, parameter matching using the two-pool exchange model produced no detectable errors until k_f^{Pi} surpassed 0.17 s^{-1}. An increase in k_f^{Pi} from 0.17 to 0.4 s^{-1} resulted in errors in the estimation of k_f^{CK}, T_1^{PCr}, and M_R^{PCr} by −1.2, 1.2, and 2.7% respectively (i.e. one dictionary step). Similarly, increase in P_i-to-ATP ratio produced no detectable errors until it surpassed 0.35. As M_R^{Pi} increased to 2.0, errors in k_f^{CK}, T_1^{PCr}, and M_R^{PCr} increased, but remained below 5%. No errors in ω^{PCr} were observed in any cases.

Sensitivity of k_f^{CK} Quantification to Selective Saturation Power

The errors introduced by not fully modeling the spillover effect of the saturation pulses are shown in Figure 2S. Each investigated method showed a power-dependent error in k_f^{CK} quantification. For CK-MRF and MT-MRS, an “optimal” saturation power was available that could obtain error-free quantification. Using a lower than “optimal” saturation power for both methods would lead to underestimation of k_f^{CK}, due to incomplete saturation of γATP. Using a higher than “optimal” saturation power led to overestimation of k_f^{CK} due to incomplete correction of the spillover on PCr. Errors in k_f^{CK} estimation by CK-MRF were comparable to conventional MT-MRS, while the FAST method showed a ~6% underestimation of k_f^{CK} throughout the range of RF power investigated. MT-MRS using the Kingsley-Monahan correction method showed least errors comparing to the other methods.

In Vivo Results

Representative spectra acquired in vivo using CK-MRF and conventional MT-MRS methods are shown in Figure 4. The corresponding fingerprints and their matched dictionary entries are also shown. For a 96-average CK-MRF acquisition, SNR of PCr in Fourier-transformed spectra typically varied from 3 to 270 from the lowest to highest flip angles (from 2.6° to 82°), and SNR of ATP varied from 0.2 to 51. In comparison, for MT-MRS measurements, SNR of PCr from a 12-average acquisition was 294 and 118 in spectra acquired without saturation and with 7-s saturation, respectively. SNR of ATP was 42 in spectra acquired without saturation. With 96 signal averages, the average inner product between an acquired fingerprint and its matching dictionary entry was 0.998 ± 0.001. The inner product between a single-averaged fingerprint and its matching dictionary entry was 0.981 ± 0.008.

Author Manuscript Author Manuscript Author Manuscript Author Manuscript

Comparison of In Vivo CK-MRF

Figure 5 shows the Bland-Altman comparison of $k_f^{\mathrm{CK}}, T_1^{\mathrm{PCr}}$, and M_R^{PCr} estimation obtained from high SNR data for both CK-MRF and MT-MRS, with group statistics summarized in Table 1. The use of CK-MRF led to a slight underestimation of k_f^{CK} with a difference of (−3.6±4.8)% ($p<0.05$). Differences in T_1^{PCr} and M_R^{PCr} estimation were insignificant with values of (0.7±5.3)% and (−1.2±5.3)%, respectively.

Compared to baseline values, both methods detected a significant post-IR increase in k_f^{CK} of ~13% ($p<0.05$). This increase was also significant compared to k_f^{CK} changes observed in control animals. Additionally, a decrease in M_R^{PCr} was observed in post-IR data from both CK-MRF and MT-MRS methods. However, only the differences detected by CK-MRF were found to be significant.

Reproducibility of In Vivo CK-MRF vs MT-MRS

Representative time courses of repeated parameter measurements by CK-MRF and MT-MRS during a data collection session at baseline are shown in Figure 6. The difference in measurement density for single-average data (Figures 6a–c) is due to the difference in acquisition time between the two methods (20 versus 150 s). Comparison between measurements made with approximately equal acquisition time (140 versus 150 s), i.e. seven averages for CK-MRF, are shown in Figures 6d–f. Parameter values obtained from 20-, 140-, and 150-s acquisition are presented in Table 2. These values did not differ significantly from those obtained from ~30-min acquisition (Table 1).

To separate the effects of inter-animal variations, the coefficient of variation (CV) for each parameter was calculated for each animal (Figure 7). Average CV of k_f^{CK} from 20-s CK-MRF acquisition was 42% of the size of the CV from 150-s MT-MRS acquisition ($p<0.05$, Figure 7a). With equal acquisition time, the CV of k_f^{CK} estimated by CK-MRF further reduced to 26% of the CV by MT-MRS. The CV of T_1^{PCr} and M_R^{PCr} estimated by CK-MRF were also significantly smaller than by MT-MRS for both 20-s and 140-s acquisition (Figure 7b–c). Finally, the CV of parameters estimated by CK-MRF was significantly smaller than that generated using FAST ($p<0.05$, Figure 7d–f). Specifically, CV of k_f^{CK} from CK-MRF was 12% of that by FAST for 20-s acquisitions.

Discussion

In this work, a novel ^{31}P CK-MRF method to quantify CK rate based on the MRF framework has been proposed. Simulation studies were used to characterize the sensitivity of CK-MRF measurements to several potential sources of errors. The accuracy and reproducibility of the CK-MRF method was evaluated *in vivo* against a conventional MT-MRS method. Previously, it has been shown in ^{31}P spectroscopic imaging that bSSFP-based approach offers a high gain of SNR per unit time with preserved coherence of magnetization[24]. In the current study, a bSSFP-type pulse sequence was used with a unique

Author Manuscript Author Manuscript Author Manuscript Author Manuscript

RF and acquisition scheme. While the interleaved saturation and acquisition scheme gave rise to MT-modulated signal evolution, the MT effect was further enhanced by the use of bSSFP-like acquisition that allowed the history of signal evolution to be preserved throughout data acquisition. In addition, the combination of inversion recovery and saturation transfer also allowed greater separation between dictionary entries. As a result, the CK-MRF method showed improved acquisition time and reproducibility for quantification of CK rate, as demonstrated by *in vivo* experiments.

It is worth noting that acquisition time and reproducibility must be considered together when evaluating the efficiency of a method. In the current study, the CK-MRF method was able to quantify k_f^{CK} *in vivo* in 20 s with a coefficient of variation of only 3.7%. Compared to the MT-MRS method, this demonstrated both an improvement in measurement reproducibility (CV for k_f^{CK} of 3.7 versus 9% for CK-MRF and MT-MRS, respectively), as well as a reduction in acquisition time (20 s versus 150 s for CK-MRF and MT-MRS, respectively). Although acquisition parameters for MT-MRS used in the current study were not optimized, it is unlikely that its acquisition time can be significantly reduced without compromising the reproducibility. The reproducibility of CK-MRF was also benchmarked in the context of equal acquisition time. CK-MRF also showed significantly reduced CV in k_f^{CK} quantification with the same acquisition time when compared to MT-MRS and FAST methods. Acquisition time for conventional MT methods can be further reduced by using a fixed T_1^{PCr} value[18,19], which was not investigated in the current study. Future investigation comparing these approaches is warranted.

The CK-MRF method may provide the potential for spatially localized CK measurement with improved efficiency. Spatial localization is a long-standing challenge for MT-MRS methods due to the additional SNR penalty for spatial encoding. Using CK-MRF, more signal averages can be achieved within the same acquisition time. Furthermore, since CK-MRF data are acquired using spectrally selective excitation, it has the advantage of allowing spatial encoding to be performed using imaging methods rather than the more time-consuming CSI methods. A previous study using conventional MT-MRS method in combination with spectrally selective excitation has demonstrated feasibility of k_f^{CK} mapping on a 7T clinical system in less than 60 min[31]. CK-MRF combined with spatial encoding may allow further reduction of the acquisition time.

The baseline k_f^{CK} and PCr-to-ATP ratio (M_R^{PCr}) obtained in this work are consistent with those reported previously[32]. The slight decrease in M_R^{PCr} after two rounds of IR is also consistent with a previous study in pig muscle subject to three rounds of IR[33]. In conjunction with the decrease in PCr, an increase in post-IR k_f^{CK} was detected by both MT-MRS and CK-MRF methods. While this increase has not been reported previously, it might be a result of the decreased PCr concentration or concentration changes in other high-energy phosphate metabolites such as ADP. Previously, McFarland et al observed increased k_f^{CK} with decreased PCr content in stimulated perfused soleus muscle[34], which was attributed to the concurrent increase in ADP concentration based on the Michaelis-Menten kinetics[35,36].

Author Manuscript Author Manuscript Author Manuscript Author Manuscript

However, studies using longer ischemic duration have observed decrease in both k_f^{CK} and PCr concentration[3,37]. The mechanisms and the relationship between ischemia duration and subsequent changes in creatine kinase kinetics need further investigation.

In the current study, several parameters, including $T_1^{\gamma\mathrm{ATP}}$, $T_2^{\gamma\mathrm{ATP}}$, T_2^{PCr}, $\Delta\omega^{\mathrm{PCr-}\gamma\mathrm{ATP}}$, linewidth, and B_1, used fixed values instead of being matched to reduce computation time and memory requirements. Insensitivity to these fixed parameters is a desirable quality for pulse sequence design for several reasons. First, it allows accurate measurement of the matched parameters without precise pilot measurements of these fixed parameters. Second, it allows a single dictionary to be computed for a particular study, despite minor inter-subject and inter-measurement variations such as in metabolite T_2 values[38]. Robustness to B_1 errors is of particular importance as many ^{31}P MRS studies are performed using surface coils with significant B_1 inhomogeneity. Our simulation results show that errors in k_f^{CK} measurement was less than 3% in the presence of ±50% error in B_1 flip angle. Further, in vivo measurements of k_f^{CK} also showed strong agreement with both MT-MRS and FAST measurements. However, our current study was performed using a saddle coil. Whether this robustness to B_1 miscalibration is sufficient for measurements using surface coils needs further investigation.

CK-MRF also showed tolerance to physiological variations such as P_i exchange rate with γATP. Simulations using values associated with resting rat skeletal muscle[39] showed no detectable errors. While P_i exchange rates with ATP may be higher in other organs or physiological conditions, simulations showed less than 5% error in k_f^{CK} measurement even with over a fivefold increase in either the rate of P_i to ATP or the concentration of P_i compared to that of resting skeletal muscle.

A limitation of the current study is that the value of $T_1^{\gamma ATP}$ was fixed rather than matched to reduce the computation time and memory requirements during parameter estimation. Unlike MT-MRS method in which $T_1^{\gamma ATP}$ does not affect the kinetics of PCr signal, in CK-MRF method, errors in fixed parameter $T_1^{\gamma ATP}$ do have the potential to cause significant errors in k_f^{CK} measurement. This error is approximately 30% the size of the error in $T_1^{\gamma ATP}$. Hence, variations in $T_1^{\gamma ATP}$ under pathophysiological conditions need to be carefully evaluated. In vivo measurement of $T_1^{\gamma ATP}$ is nontrivial, especially for the current CK-MRF method because the magnetization of αATP and βATP is not disturbed. Hence, the intramolecular NOE effects between γATP and αATP and between γATP and βATP also need to be considered. While this may be addressed by expanding the Bloch-McConnell equation to include these effects through additional exchanging pools[6], substantial validation of such an approach would be needed to evaluate its potential accuracy and robustness.

Another limitation of the proposed CK-MRF method is that the data acquisition scheme using selective RF excitation only samples PCr and γATP magnetization. As a result, other information that are available in conventional ^{31}P MT-MRS methods, such as P_i-to-ATP exchange, pH and PDE and ADP concentrations, cannot be obtained from CK-MRF data.

Author Manuscript Author Manuscript Author Manuscript Author Manuscript

While pH and metabolite concentrations can be obtained from a conventional ^{31}P spectrum, the quantification of P_i-to-ATP exchange is much more challenging due to the low concentration of P_i. On the other hand, it has been shown that the P_i-to-ATP exchange is more relevant in diseases that affect skeletal muscle[9]. The development of a fast and robust MRF method that also enables the quantification of the P_i-to-ATP exchange should be a priority for future work.

Continuous wave RF pulses were used in the CK-MRF method to perform selective saturation. The spillover effect on PCr was partially accounted for by applying contralateral saturation pulses. Simulations show that the errors introduced by such an approach were power dependent, and the errors were comparable to those observed in conventional MT-MRS method. The observed 3.6% underestimation in k_f^{CK} by CK-MRF is consistent with the bias expected between the two methods for a saturation power between 11 to 14 Hz. With improved mapping of the B_1 field, these errors may be correctable by using explicit methods[29], or by building saturation power into the dictionary as an additional fixed or matched parameter. Alternatively, continuous wave RF may be replaced by another saturation pulse such as BISTRO[40] with reduced spillover effect.

To reduce computation time and memory requirements, the current dictionary choice of matched parameters and parameter resolution was selected as an acceptable tradeoff between potential errors size and dictionary computation and memory size. Simulation results showed that the current dictionary resolution resulted in the nearest-neighbor match for matched parameters, with the exception of T_1^{PCr}, where the next-nearest-neighbor may also be matched. This result implies that the accuracy of parameter match can be further improved by using a dictionary resolution with a finer resolution.

In conclusion, this work is a first step towards quantifying phosphate metabolism using the MRF framework. CK-MRF was able to significantly increase measurement reproducibility compared to the conventional ^{31}P MT-MRS method while exhibiting robustness to several error sources. The improvement in measurement efficiency may be leveraged in several ways, such as more accurate measurements made in equivalent experimental time, or reduced experimental time with equivalent measurement accuracy, allowing for new applications of ^{31}P studies on tissue metabolism.

Supplementary Material

Refer to Web version on PubMed Central for supplementary material.

Acknowledgments

Sponsors: This work was supported by grants from the National Institute of Health R21-HL126215, R01-HL73315, F30-HL124894, T32-EB007509, TL1-TR000441, T32-GM007250, R01-HL94557, R01-DK98503, and from the National Science Foundation CBET1553441.

This work made use of the High Performance Computing Resource in the Core Facility for Advanced Research Computing at Case Western Reserve University.

Author Manuscript Author Manuscript Author Manuscript Author Manuscript

Abbreviations

^{31}P	phosphorus-31
ACQ-PCr	acquisition block with PCr excitation
ACQ-γATP	acquisition block with γATP excitation
ADP	adenosine diphosphate
ATP	adenosine triphosphate
bSSFP	balanced steady-state free precession
CK	creatine kinase
CK-MRF	creatine kinase encoded magnetic resonance fingerprinting
CSI	chemical shift imaging
CV	coefficient of variation
FAST	four angle saturation transfer
FID	free induction decay
LW	linewidth
NOE	nuclear Overhauser effect
MRF	magnetic resonance fingerprinting
MT	magnetization transfer
MT-MRS	magnetization-transfer encoded magnetic resonance spectroscopy
PCr	phosphocreatine
P_i	inorganic phosphate
SAT-γATP	selective saturation block applied on γATP resonance
SAT-CNTL	selective saturation block applied contralateral to γATP resonance relative to phosphocreatine resonance
SD	standard deviation
TR	repetition time

References

1. El-Sharkawy A-MM, Gabr RE, Schär M, Weiss RG, Bottomley PA. Quantification of human high-energy phosphate metabolite concentrations at 3 T with partial volume and sensitivity corrections. NMR Biomed. 2013; 26(11):1363–1371. [PubMed: 23729378]

Author Manuscript Author Manuscript Author Manuscript Author Manuscript

2. Neubauer S, Horn M, Cramer M, Harre K, Newell JB, Peters W, Pabst T, Ertl G, Hahn D, Ingwall JS, Kochsiek K. Myocardial phosphocreatine-to-ATP ratio is a predictor of mortality in patients with dilated cardiomyopathy. Circulation. 1997; 96(7):2190–2196. [PubMed: 9337189]

3. Bittl JA, Balschi JA, Ingwall JS. Contractile failure and high-energy phosphate turnover during hypoxia: 31P-NMR surface coil studies in living rat. Circ Res. 1987; 60(6):871–878. [PubMed: 2954720]

4. Koretsky AP, Wang S, Murphy-Boesch J, Klein MP, James TL, Weiner MW. 31P NMR spectroscopy of rat organs, in situ, using chronically implanted radiofrequency coils. Proc Natl Acad Sci U S A. 1983; 80(24):7491–7495. [PubMed: 6584867]

5. Bittl JA, Ingwall JS. Reaction rates of creatine kinase and ATP synthesis in the isolated rat heart. A 31P NMR magnetization transfer study. J Biol Chem. 1985; 260(6):3512–3517. [PubMed: 3972835]

6. Ren J, Yang B, Sherry aD, Malloy CR. Exchange kinetics by inversion transfer: integrated analysis of the phosphorus metabolite kinetic exchanges in resting human skeletal muscle at 7 T. Magn Reson Med. 2015; 73(4):1359–1369. [PubMed: 24733433]

7. Degani H, Laughlin M, Campbell S, Shulman RG. Kinetics of creatine kinase in heart: a 31P NMR saturation- and inversion-transfer study. Biochemistry. 1985; 24(20):5510–5516. [PubMed: 4074712]

8. Leibfritz D, Dreher W. Magnetization transfer MRS. NMR Biomed. 2001; 14(2):65–76. [PubMed: 11320534]

9. Befroy DE, Rothman DL, Petersen KF, Shulman GI. ^{31}P-magnetization transfer magnetic resonance spectroscopy measurements of in vivo metabolism. Diabetes. 2012; 61(11):2669–2678. [PubMed: 23093656]

10. Balaban RS, Kantor HL, Ferretti JA. In vivo flux between phosphocreatine and adenosine triphosphate determined by two-dimensional phosphorous NMR. J Biol Chem. 1983; 258(21): 12787–12789. [PubMed: 6630206]

11. Kingsley-Hickman PB, Sako EY, Mohanakrishnan P, Robitaille PM, From AH, Foker JE, Uđurbil K. 31P NMR studies of ATP synthesis and hydrolysis kinetics in the intact myocardium. Biochemistry. 1987; 26(23):7501–7510. [PubMed: 3427090]

12. Robitaille PM, Merkle H, Sako E, Lang G, Clack RM, Bianco R, From AH, Foker J, Uđurbil K. Measurement of ATP synthesis rates by 31P-NMR spectroscopy in the intact myocardium in vivo. Magn Reson Med. 1990; 15(1):8–24. [PubMed: 2374502]

13. Kingsley-Hickman PB, Sako EY, Uđurbil K, From AH, Foker JE. 31P NMR measurement of mitochondrial uncoupling in isolated rat hearts. J Biol Chem. 1990; 265(3):1545–1550. [PubMed: 2136855]

14. Ingwall JS. Phosphorus nuclear magnetic resonance spectroscopy of cardiac and skeletal muscles. Am J Physiol. 1982; 242(5):H729–44. [PubMed: 7044148]

15. Lei H, Zhu X, Zhang X, Ugurbil K, Chen W. In vivo 31P magnetic resonance spectroscopy of human brain at 7 T: an initial experience. Magn Reson Med. 2003; 49(2):199–205. [PubMed: 12541238]

16. Bottomley PA, Ouwerkerk R, Lee RF, Weiss RG. Four-angle saturation transfer (FAST) method for measuring creatine kinase reaction rates in vivo. Magn Reson Med. 2002; 47(5):850–863. [PubMed: 11979563]

17. Schär M, El-Sharkawy A-MM, Weiss RG, Bottomley PA. Triple repetition time saturation transfer (TRiST) 31P spectroscopy for measuring human creatine kinase reaction kinetics. Magn Reson Med. 2010; 63(6):1493–1501. [PubMed: 20512852]

18. Schär M, Gabr RE, El-Sharkawy A-MM, Steinberg A, Bottomley PA, Weiss RG. Two repetition time saturation transfer (TwiST) with spill-over correction to measure creatine kinase reaction rates in human hearts. J Cardiovasc Magn Reson. 2015; 17(1):70. [PubMed: 26253320]

19. Xiong Q, Du F, Zhu X, Zhang P, Suntharalingam P, Ippolito J, Kamdar FD, Chen W, Zhang J. ATP production rate via creatine kinase or ATP synthase in vivo: a novel superfast magnetization saturation transfer method. Circ Res. 2011; 108(6):653–663. [PubMed: 21293002]

20. Ma D, Gulani V, Seiberlich N, Liu K, Sunshine JL, Duerk JL, Griswold MA. Magnetic resonance fingerprinting. Nature. 2013; 495(7440):187–192. [PubMed: 23486058]

Author Manuscript Author Manuscript Author Manuscript Author Manuscript

21. Jiang Y, Ma D, Seiberlich N, Gulani V, Griswold Ma. MR fingerprinting using fast imaging with steady state precession (FISP) with spiral readout. Magn Reson Med. 2015; 74(6):1621–1631. [PubMed: 25491018]
22. Chen Y, Jiang Y, Pahwa S, Ma D, Lu L, Twieg MD, Wright KL, Seiberlich N, Griswold MA, Gulani V. MR Fingerprinting for Rapid Quantitative Abdominal Imaging. Radiology. 2016; 279(1):278–286. [PubMed: 26794935]
23. Hamilton JI, Jiang Y, Chen Y, Ma D, Lo WC, Griswold M, Seiberlich N. MR fingerprinting for rapid quantification of myocardial T1, T2, and proton spin density. Magn Reson Med. 2016:0.
24. Speck O, Scheffler K, Hennig J. Fast 31P chemical shift imaging using SSFP methods. Magn Reson Med. 2002; 48(4):633–639. [PubMed: 12353280]
25. Deshpande VS, Chung Y-C, Zhang Q, Shea SM, Li D. Reduction of transient signal oscillations in true-FISP using a linear flip angle series magnetization preparation. Magn Reson Med. 2003; 49(1):151–157. [PubMed: 12509831]
26. Deoni SCL, Rutt BK, Jones DK. Investigating exchange and multicomponent relaxation in fully-balanced steady-state free precession imaging. J Magn Reson Imaging. 2008; 27(6):1421–1429. [PubMed: 18504765]
27. Nabuurs C, Huijbregts B, Wieringa B, Hilbers CW, Heerschap A. 31P saturation transfer spectroscopy predicts differential intracellular macromolecular association of ATP and ADP in skeletal muscle. J Biol Chem. 2010; 285(51):39588–39596. [PubMed: 20884612]
28. Bashir A, Gropler R. Reproducibility of creatine kinase reaction kinetics in human heart: a (31) P time-dependent saturation transfer spectroscopy study. NMR Biomed. 2014; 27(6):663–671. [PubMed: 24706347]
29. Kingsley PB, Monahan WG. Corrections for off-resonance effects and incomplete saturation in conventional (two-site) saturation-transfer kinetic measurements. Magn Reson Med. 2000; 43(6): 810–819. [PubMed: 10861875]
30. Liu Y, Mei X, Li J, Lai N, Yu X. Mitochondrial function assessed by 31P MRS and BOLD MRI in non-obese type 2 diabetic rats. Physiol Rep. 2016; 4(15):e12890. [PubMed: 27511984]
31. Parasoglou P, Xia D, Chang G, Convit A, Regatte RR. Three-dimensional mapping of the creatine kinase enzyme reaction rate in muscles of the lower leg. NMR Biomed. 2013; 26(9):1142–1151. [PubMed: 23436474]
32. Shoubridge EA, Bland JL, Radda GK. Regulation of creatine kinase during steady-state isometric twitch contraction in rat skeletal muscle. BBA - Mol Cell Res. 1984; 805(1):72–78.
33. Pang CY, Neligan P, Xu H, He W, Zhong A, Hopper R, Forrest CR. Role of ATP-sensitive K+ channels in ischemic preconditioning of skeletal muscle against infarction. Am J Physiol. 1997; 273(1 Pt 2):H44–51. [PubMed: 9249473]
34. McFarland EW, Kushmerick MJ, Moerland TS. Activity of creatine kinase in a contracting mammalian muscle of uniform fiber type. Biophys J. 1994; 67(5):1912–1924. [PubMed: 7858128]
35. Morrison JF, Cleland WW. Isotope exchange studies of the mechanism of the reaction catalyzed by adenosine triphosphate: creatine phosphotransferase. J Biol Chem. 1966; 241(3):673–683. [PubMed: 5908134]
36. Schimerlik MI, Cleland WW. Inhibition of creatine kinase by chromium nucleotides. J Biol Chem. 1973; 248(24):8418–8423. [PubMed: 4797017]
37. Neubauer S, Hamman BL, Perry SB, Bittl JA, Ingwall JS. Velocity of the creatine kinase reaction decreases in postischemic myocardium: a 31P-NMR magnetization transfer study of the isolated ferret heart. Circ Res. 1988; 63(1):1–15. [PubMed: 3383370]
38. Bogner W, Chmelik M, Schmid AI, Moser E, Trattnig S, Gruber S. Assessment of (31)P relaxation times in the human calf muscle: a comparison between 3 T and 7 T in vivo. Magn Reson Med. 2009; 62(3):574–582. [PubMed: 19526487]
39. van den Broek NM, Ciapaite J, Nicolay K, Prompers JJ. Comparison of in vivo postexercise phosphocreatine recovery and resting ATP synthesis flux for the assessment of skeletal muscle mitochondrial function. AJP Cell Physiol. 2010; 299(5):C1136–C1143.
40. Luo Y, de Graaf RA, DelaBarre L, Tannús A, Garwood M. BISTRO: an outer-volume suppression method that tolerates RF field inhomogeneity. Magn Reson Med. 2001; 45(6):1095–1102. [PubMed: 11378888]

Author Manuscript Author Manuscript Author Manuscript Author Manuscript

Appendix

Signal evolutions in response to a pulse sequence were simulated using the Bloch-McConnell equations[16,26]. The matrix form of the Bloch-McConnell equations can be expressed as:

$$\frac{d}{dt}M = AM + C \quad \text{[A1]}$$

where M is a vector that describes the evolution of the transverse and longitudinal magnetization. For two exchanging species PCr and γATP, M is defined as:

$$M = [\ M_x^{\mathrm{PCr}} \quad M_y^{\mathrm{PCr}} \quad M_z^{\mathrm{PCr}} \quad M_x^{\gamma\mathrm{ATP}} \quad M_y^{\gamma\mathrm{ATP}} \quad M_z^{\gamma\mathrm{ATP}}\ ]^T \quad \text{[A2]}$$

C is a vector that describes the steady-state magnetization weighted by the longitudinal relaxation, i.e.,

$$C = \left[\ 0 \quad 0 \quad \frac{M_0^{\mathrm{PCr}}}{T_1^{\mathrm{PCr}}} \quad 0 \quad 0 \quad \frac{M_0^{\gamma\mathrm{ATP}}}{T_1^{\gamma\mathrm{ATP}}}\ \right]^T \quad \text{[A3]}$$

where M_0^{PCr} and $M_0^{\gamma\mathrm{ATP}}$ are the steady-state magnetization and T_1^{PCr} and $T_1^{\gamma\mathrm{ATP}}$ are the longitudinal relaxation time for PCr and γATP, respectively. A is a matrix that describes the precession, relaxation, and magnetization exchange between PCr and γATP. For PCr and γATP with resonance frequencies $\omega^{\mathrm{PCr}}$and $\omega^{\gamma\mathrm{ATP}}$ observed in a rotating frame of frequency ω, A matrix can be expressed as:

$$A = \begin{bmatrix}
-\frac{1}{T_2^{\mathrm{PCr}}} - k_f^{\mathrm{CK}} & \Delta\omega^{\mathrm{PCr}} + \Delta\omega_0 & & k_r^{\mathrm{CK}} & & \\
-\Delta\omega^{\mathrm{PCr}} - \Delta\omega_0 & -\frac{1}{T_2^{\mathrm{PCr}}} - k_f^{\mathrm{CK}} & & & k_r^{\mathrm{CK}} & \\
 & & -\frac{1}{T_1^{\mathrm{PCr}}} - k_f^{\mathrm{CK}} & & & k_r^{\mathrm{CK}} \\
k_f^{\mathrm{CK}} & & & -\frac{1}{T_2^{\gamma ATP}} - k_r^{\mathrm{CK}} & \Delta\omega^{\gamma\mathrm{ATP}} + \Delta\omega_0 & \\
 & k_f^{\mathrm{CK}} & & -\Delta\omega^{\gamma\mathrm{ATP}} - \Delta\omega_0 & -\frac{1}{T_2^{\gamma\mathrm{ATP}}} - k_r^{\mathrm{CK}} & \\
 & & k_f^{\mathrm{CK}} & & & -\frac{1}{T_1^{\gamma\mathrm{ATP}}} - k_r^{\mathrm{CK}}
\end{bmatrix} \quad \text{[A4]}$$

where T_2^{PCr} and $T_2^{\gamma\mathrm{ATP}}$ are the transverse relaxation time of PCr and γATP, respectively. $\Delta\omega^{\mathrm{PCr}}$ and $\Delta\omega^{\gamma\mathrm{ATP}}$ are the difference between the resonance frequency of PCr (ω^{PCr}) and γATP ($\omega^{\gamma\mathrm{ATP}}$) from the frequency of the rotating frame (ω.), i.e., $\Delta\omega^{\mathrm{PCr}} = \omega^{\mathrm{PCr}} - \omega$ and $\Delta\omega^{\gamma\mathrm{ATP}} = \omega^{\gamma\mathrm{ATP}} - \omega$. $\Delta\omega_0$ is the frequency dispersion term used to account for B_0 field

Author Manuscript Author Manuscript Author Manuscript Author Manuscript

inhomogeneity. k_f^{CK} and k_r^{CK} are the forward and reverse exchange rate from PCr to γATP, respectively. Chemical equilibrium was assumed for all simulations such that:

$$k_r^{\mathrm{CK}}=k_f^{\mathrm{CK}}\frac{M_0^{\mathrm{PCr}}}{M_0^{\gamma ATP}} \quad [A5]$$

Starting from a fully relaxed spin system, signal evolutions in response to a pulse sequence were simulated by iteratively solving for M in discrete time steps (Δt) using the discrete time solution for Equation A1:

$$M^{N+1}=e^{A\Delta t}M^N+(e^{A\Delta t}-I)A^{-1}C \quad [A6]$$

where M^N and M^{N+1} are magnetization vectors before and after an iteration.

RF pulses were modeled as discretized instantaneous rotations about the x- and y-axis of the rotating frame:

$$M^+=R_x(\alpha_x)R_y(\alpha_y)M^- \quad [A7]$$

where M^- and M^+ are the magnetization vector before and after the RF pulse, and $R_x(\alpha_x)$ and $R_y(\alpha_y)$ are the rotation matrix about the x- and y-axis with flip angles α_x and α_y, respectively, i.e.,

$$R_x(\alpha_x)=\begin{bmatrix} 1 & & & & & \\ & \cos\alpha_x & -\sin\alpha_x & & & \\ & \sin\alpha_x & \cos\alpha_x & & & \\ & & & 1 & & \\ & & & & \cos\alpha_x & -\sin\alpha_x \\ & & & & \sin\alpha_x & \cos\alpha_x \end{bmatrix} \quad [A8]$$

$$R_y(\alpha_y)=\begin{bmatrix} \cos\alpha_y & & -\sin\alpha_y & & & \\ & 1 & & & & \\ \sin\alpha_y & & \cos\alpha_y & & & \\ & & & \cos\alpha_y & & -\sin\alpha_y \\ & & & & 1 & \\ & & & \sin\alpha_y & & \cos\alpha_y \end{bmatrix} \quad [A9]$$

Once M is solved, the FID signal, i.e., the transverse magnetization $M_\perp$, was computed as

Author Manuscript Author Manuscript Author Manuscript Author Manuscript

$$M_{\perp}=\begin{bmatrix} M_{\perp}^{\mathrm{PCr}} \\ M_{\perp}^{\gamma\,\mathrm{ATP}} \end{bmatrix}=\begin{bmatrix} M_{x}^{\mathrm{PCr}}+iM_{y}^{\mathrm{PCr}} \\ M_{x}^{\gamma\,\mathrm{ATP}}+iM_{y}^{\gamma\,\mathrm{ATP}} \end{bmatrix} \quad [A10]$$

To account for the effects of B_0 inhomogeneity, simulations were repeated with 51 different values of $\Delta\omega_0$ ranging from −75 to 75 Hz with a uniform resolution of 3 Hz. The total signal, $S(t)$, was calculated as the weighted sum of 51 simulations:

$$S(t)=\sum\nolimits_{\Delta\omega_0} W(\Delta\omega_0)M_{\perp}(t,\Delta\omega_0) \quad [A11]$$

where $W(\Delta\omega_0)$ is the corresponding weight for a frequency component derived from a Lorentzian lineshape with a linewidth LW:

$$W(\Delta\omega_0)=\frac{\mathrm{LW}^2}{(\Delta\omega_0)^2+\mathrm{LW}^2} \quad [A12]$$

Author Manuscript Author Manuscript Author Manuscript Author Manuscript

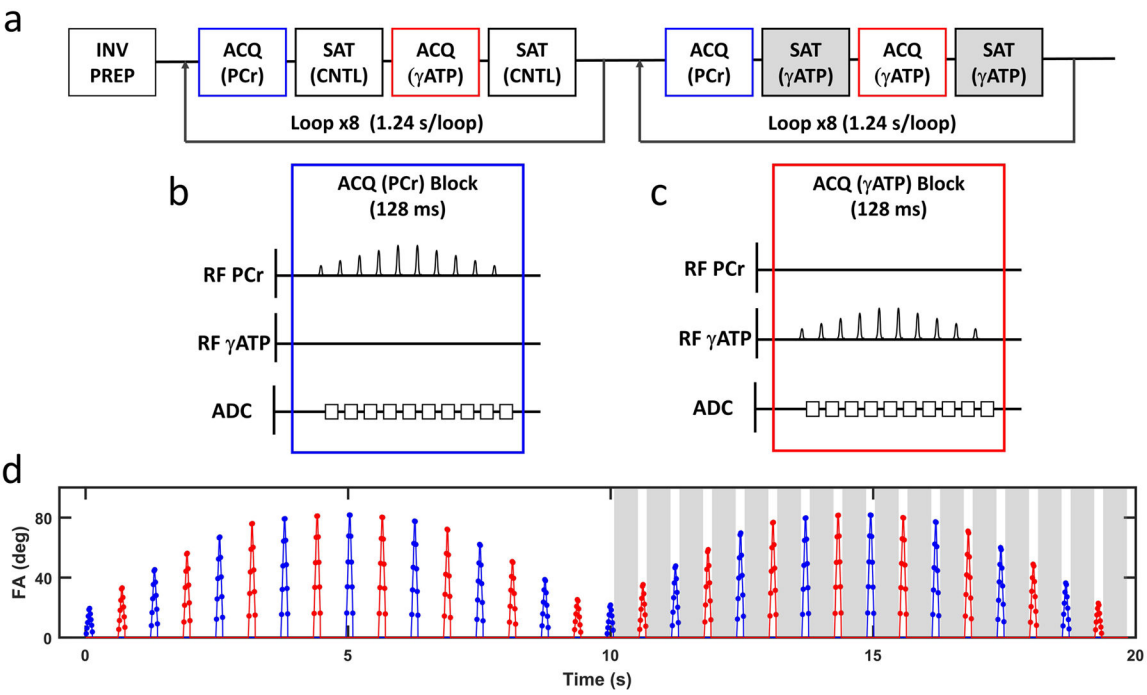

Figure 1. Sequence design

a. Schematic of the CK-MRF pulse sequence. ACQ (PCr) and ACQ (γATP) are acquisition blocks for PCr and γATP, respectively. SAT (CNTL) and SAT (γATP) are contralateral and γATP saturation blocks, respectively. ACQ (PCr) and ACQ (γATP) used Gaussian excitation pulses, while SAT (CNTL) and SAT (γATP) used continuous wave RF pulses. **b** and **c.** Pulse sequence diagrams for one block of ACQ (PCr) (b) and ACQ (γATP) (c). **d.** Timing and nominal flip angles of all excitation pulses. Blue and red colors indicate PCr and γATP excitation, respectively. Grey shaded areas indicate γATP saturation.

Author Manuscript Author Manuscript Author Manuscript Author Manuscript

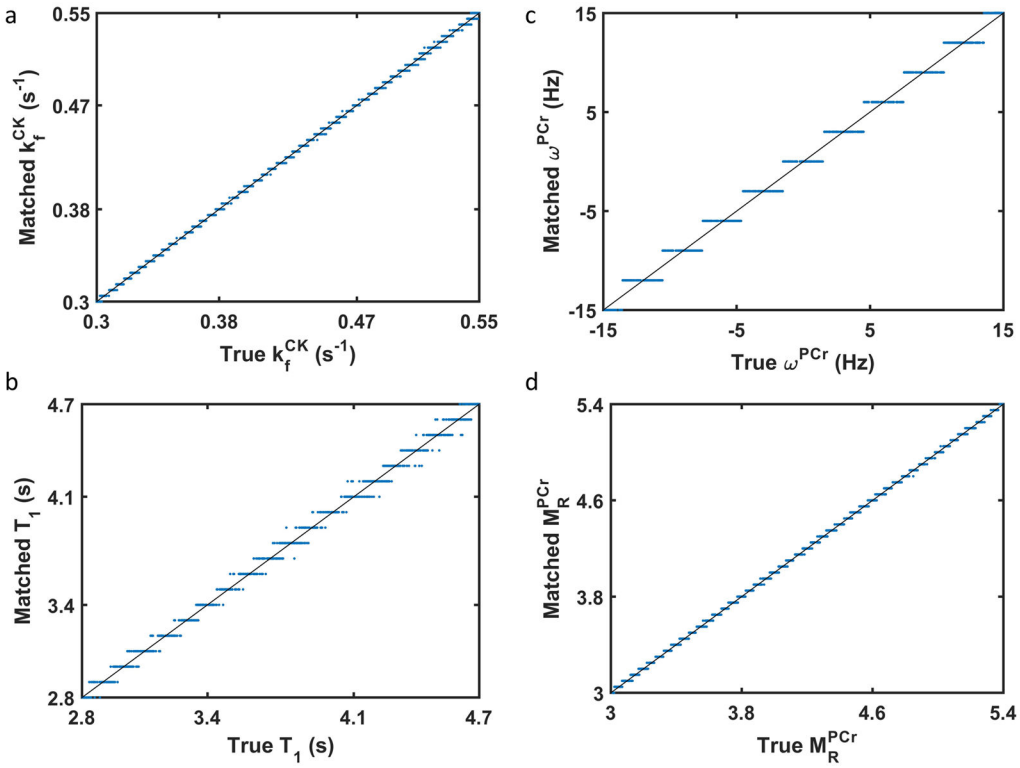

Figure 2. Comparison of dictionary matched values with the ground truth values

For each fingerprint generated using a random set of values for the four parameters to be determined, its dictionary matched parameter value for k_f^{CK} (a), T_1^{PCr} (b), ω^{PCr} (c), and M_R^{PCr} (d) is plotted against its corresponding true value. Lines of identity are included in each plot.

Author Manuscript Author Manuscript Author Manuscript Author Manuscript

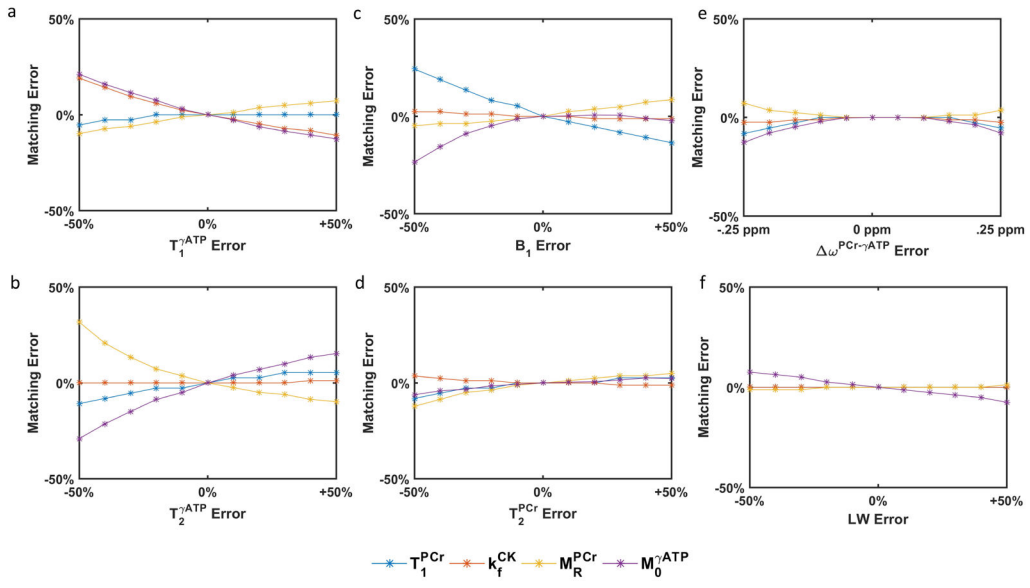

Figure 3.

Errors in matched parameters k_f^{CK}, T_1^{PCr}, M_R^{PCr}, and $M_0^{\gamma\mathrm{ATP}}$ caused by using values for fixed parameters that differ from those assumed when generating the dictionary: $T_1^{\gamma\mathrm{ATP}}$ (a), $T_2^{\gamma\mathrm{ATP}}$ (b), B_1 (c), T_2^{PCr} (d), $\Delta\omega^{\mathrm{PCr-}\gamma\mathrm{ATP}}$ (e), and LW (f).

Author Manuscript Author Manuscript Author Manuscript Author Manuscript

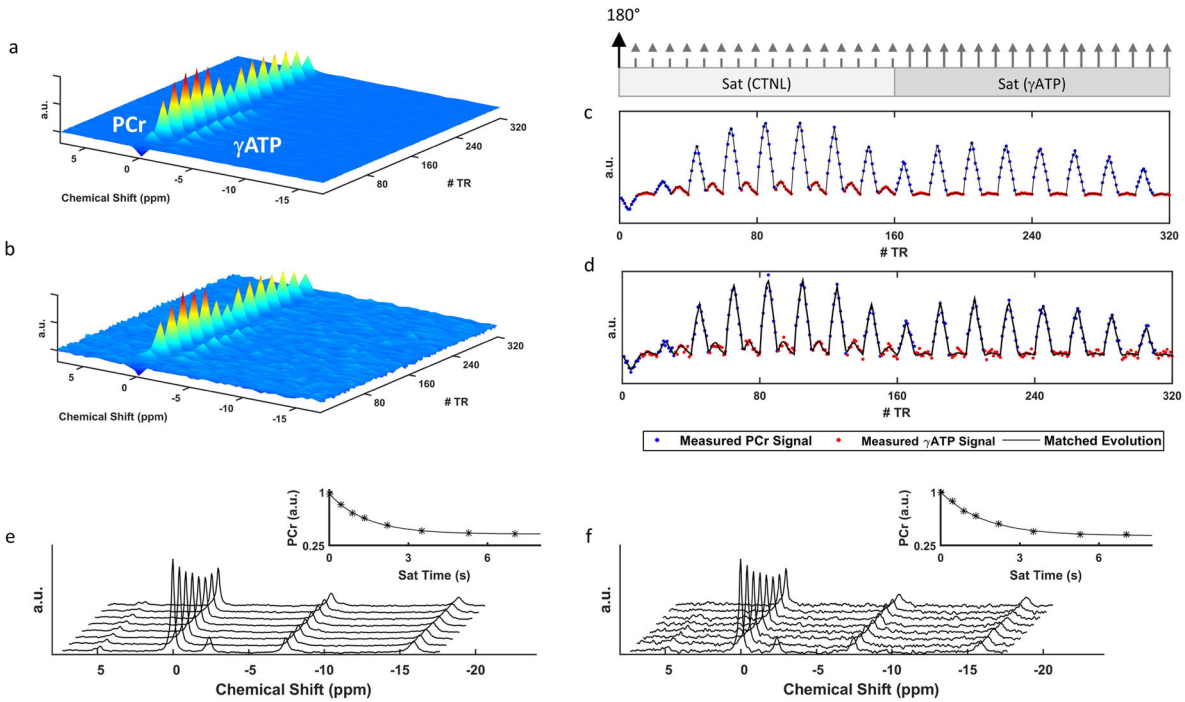

Figure 4. Representative *in vivo* CK-MRF spectra and fingerprints

a and **b**. ^{31}P spectra with 96 (a) and single (b) signal average(s). **c** and **d**. The corresponding fingerprints and their dictionary matches from 96 (c) and single (d) signal average(s). Blue and red data points represent PCr and γATP peaks, respectively. Relative timings for inversion and saturation pulses are indicated at the top. Dashed and solid arrows indicate contralateral and γATP saturation pulses, respectively. **e** and **f**. ^{31}P spectra from 12 (e) and single (f) signal average(s) by MT-MRS. Results of the corresponding curve fitting to PCr signal are shown in the insets.

Author Manuscript Author Manuscript Author Manuscript Author Manuscript

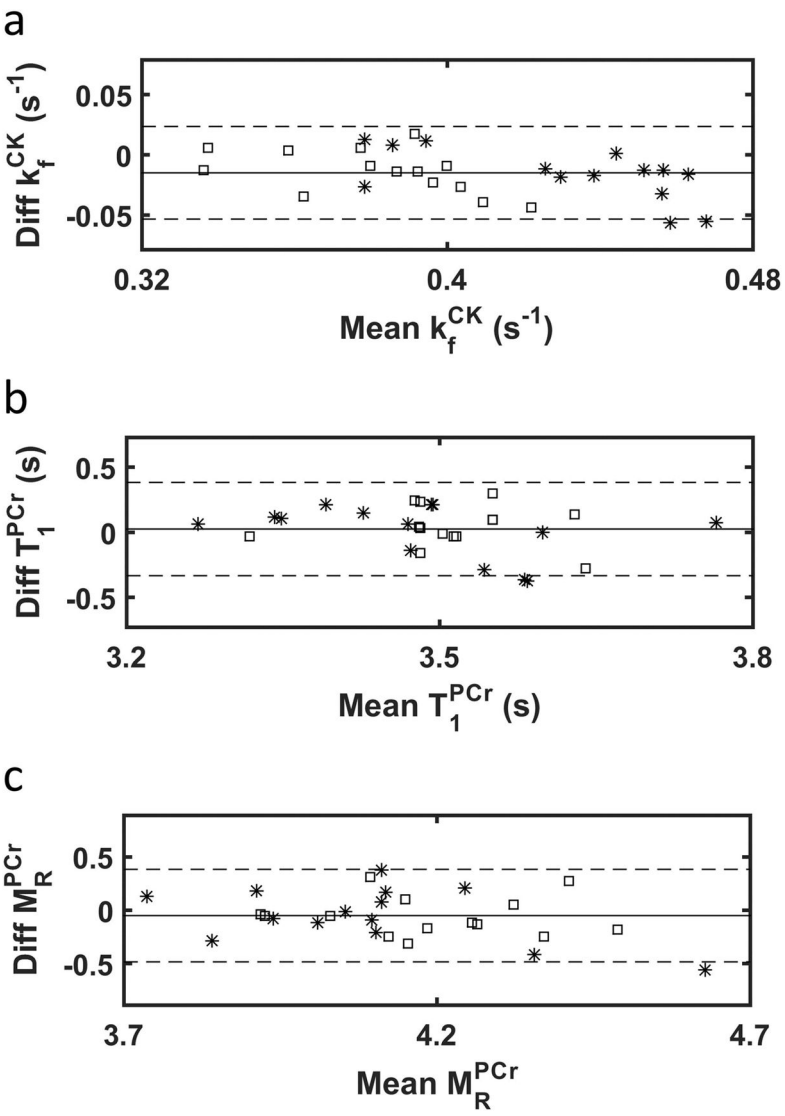

Figure 5. Comparison between parameter measurements by CK-MRF and MT-MRS

Bland-Altman plots are shown for k_f^{CK} (a), T_1^{PCr} (b), and M_R^{PCr} (c). Squares indicate pre-IR data and stars indicate post-IR data. Solid lines indicate mean differences and dashed lines indicate limits of agreement.

Author Manuscript Author Manuscript Author Manuscript Author Manuscript

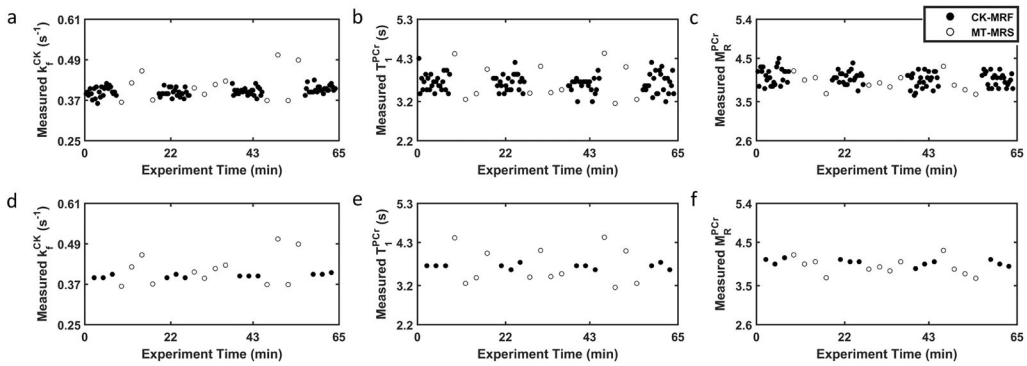

Figure 6. Repeated parameter measurements for reproducibility assessment

Sequentially acquired CK-MRF (filled circles) and MT-MRS (open circles) measurements during a data collection session are shown. **a–c.** k_f^{CK} (a), T_1^{PCr} (b), and M_R^{PCr} (c) estimation obtained from single-average data for both CK-MRF (20-s acquisition) and MT-MRS (150-s acquisition). **d–f.** k_f^{CK} (d), T_1^{PCr} (e), and M_R^{PCr} (f) estimation obtained from 7 signal averages for CK-MRF (140-s acquisition) and single average for MR-MRS (150-s acquisition).

Author Manuscript Author Manuscript Author Manuscript Author Manuscript

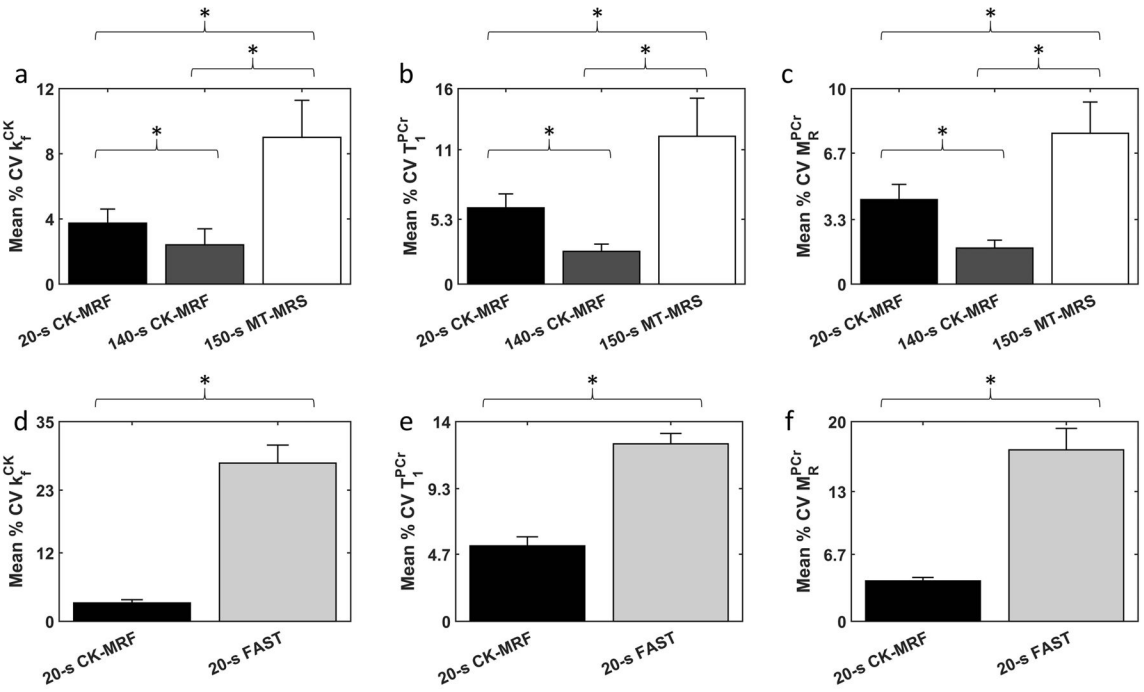

Figure 7. Reproducibility of parameter estimation

Coefficient of variation (CV, defined as SD divided by the mean of the measurements) was compared between CK-MRF and MT-MRS methods (a–c) and between CK-MRF and FAST methods (d–f), for parameters k_f^{CK} (a, b), T_1^{PCr} (c, d), and M_R^{PCr} (e, f). Acquisition times denoted represent time spent for a single measurement, including all signal averages but excluding dummy and control scans. Column height and error bars represent mean and SD of CV across animals. All comparisons are statistically significant ($p<0.05$).

Author Manuscript Author Manuscript Author Manuscript Author Manuscript

Table 1

Summary of Estimated Parameter Values Pre-IR and Post-IR (n=17)

		Acq Time (min)	Signal Averages	k_f^{CK} (s^{-1})	T_1^{PCr} (s)	M_R^{PCr}
Pre-IR	MT-MRS	30	12	0.39 ± 0.03	3.49 ± 0.11	4.22 ± 0.20
	CK-MRF	32	96	0.38 ± 0.02 *	3.54 ± 0.11	4.16 ± 0.19
Post-IR	MT-MRS	20	8	0.44 ± 0.04 †	3.48 ± 0.19	4.11 ± 0.30
	CK-MRF	16	48	0.42 ± 0.03 *†	3.49 ± 0.13	4.07 ± 0.19 †

* p<0.05, MT-MRS versus CK-MRF

† p<0.05, Pre-IR versus Post IR

NMR Biomed. Author manuscript; available in PMC 2018 December 01.

Author Manuscript Author Manuscript Author Manuscript Author Manuscript

Table 2

Estimated Parameters in Reproducibility Study

		Acq Time (s)	Signal Averages	k_f^{CK} (s^{-1})	T_1^{PCr} (s)	M_R^{PCr}
CK-MRF versus MT-MRS (n=17)	MT-MRS	150	1	0.40 ± 0.04	3.53 ± 0.44	4.22 ± 0.38
	CK-MRF	20	1	0.38 ± 0.03	3.57 ± 0.25	4.17 ± 0.25
	CK-MRF	140	7	0.38 ± 0.02	3.57 ± 0.13	4.16 ± 0.19
CK-MRF Versus FAST (n=7)	FAST	20	5	0.38 ± 0.11	2.63 ± 0.34	4.52 ± 0.85
	CK-MRF	20	1	0.38 ± 0.02	3.57 ± 0.21	4.20 ± 0.20

NMR Biomed. Author manuscript; available in PMC 2018 December 01.